Weierstraß-Institut
für Angewandte Analysis und Stochastik

im Forschungsverbund Berlin e.V.

Preprint ISSN 0946 – 8633

High Order Central Schemes Applied to Relativistic Multicomponent Flows

Shamsul Qamar

submitted: 2nd October 2003

Weierstrass Institute
for Applied Analysis
and Stochastics
Mohrenstrasse 39
10117 Berlin
Germany
E-Mail: qamar@wias-berlin.de

No. 875
Berlin 2003

2000 *Mathematics Subject Classification.* 65M99, 65Y20.

Key words and phrases. multicomponent flows, relativistic Euler equations, central schemes, higher order accuracy.

Edited by
Weierstraß-Institut für Angewandte Analysis und Stochastik (WIAS)
Mohrenstraße 39
D — 10117 Berlin
Germany

Fax: + 49 30 2044975
E-Mail: preprint@wias-berlin.de
World Wide Web: http://www.wias-berlin.de/

Abstract

The dynamics of inviscid multicomponent relativistic fluids may be modelled by the relativistic Euler equations, augmented by one (or more) additional species equation (s). We use high-resolution central schemes to solve these equations. The equilibrium states for each component are coupled in space and time to have a common temperature and velocity. The current schemes can handle strong shocks and the oscillations near the interfaces are negligible, which usually happens in the multicomponent flows. The schemes also guarantee the exact mass conservation for each component and the exact conservation of total momentum and energy in the whole particle system. The central schemes are robust, reliable, compact and easy to implement. Several one- and two-dimensional numerical test cases are included in this paper, which validate the application of these schemes to relativistic multicomponent flows.

1 Introduction

In recent years relativistic gas dynamics plays an important role in areas of astrophysics, high energy particle beams, high energy nuclear collisions, and free-electron laser technology. The equations that describe the relativistic gas dynamics are highly nonlinear. For the practical problems it is difficult to solve these equations analytically, therefore numerical solutions are persued. Several numerical methods for solving relativistic gas dynamics have been reported. All these methods are mostly developed out of the existing reliable methods for solving the Euler equations of nonrelativistic or Newtonian gas dynamics.

The first attempt to solve the equations of relativistic gas dynamics (RGD) was made by Wilson [33, 34] using an Eulerian explicit finite difference code with monotonic transport. The code relies on artificial viscosity technique [25] to handle shock wave. Despite of its popularity it truned out to be unable to accuratly describe the extremly relativistic flows, see [2]. In mid eighties, Norman and Winkler [26] proposed a reformulation of the difference equations with artificial viscosity consistent with relativistic dynamics of non-perfect fluids. Dean et al [4] used flux correcting algorithms for RGD equations in context of heavy ion collisions.

A good introduction about the recent methods applied to RGD can be found in the review article of Martí and Müller [23]. Some popular methods which are extended for RGD and are also discussed in [23] are, Rao methods [28] used by Eulderink et. al [6, 7], PPM method [3] by Martí and Müller [21], Glimm's methods [10] by Wen et. al [32], HLL method [11]

by Schneider et. al [30], Marquina flux formula [5] by Martí et. al [20, 22] and relativistic beam scheme [29] by Yang et. al [38].

The development of numerical methods for the non-relativistic multicomponent flows have attracted much attention in the past years, see for example Fedkiw et. al [8, 9], Karni [14, 15, 16], Karni and Quirk [27], Marquina and Nulet [19]. Xu [36] used BGK-based gas-kinetic schemes to solve multicomponent flow, while Lian and Xu [18] used the same scheme in order to solve the multicompment flows with chemical reactions.

This paper is an extension of the relativistic Euler equations to multi-component flows. We use high-resolution nonoscillatory central schemes of Nessyahu and Tadmor [24] as well as Jiang and Tadmor [13] to solve these Euler equations. In this study we consider only two-components flow, however the extension to further components will result in addition of continuity equation for the corresponding species. The central schemes are predictor-corrector methods which consists of two steps: starting with given cell averages, we first predict pointvalues which are based on nonoscillatory piecewise-linear reconstructions from the cell averages; at the second corrector step, we use staggered averaging, together with the predicted midvalues, to realize the evolution of these averages. This results in a second-order, nonoscillatory central scheme.

These second order accuracy of these schemes are based on MUSCL-type reconstruction. Like upwind schemes, the reconstructed piecewise-polynomials used by the central schemes, also make use of non-linear limiters which guarantee the overall non-oscillatory nature of the approximate solution. But unlike the upwind schemes, central scheme do not require the intricate and time-consuming (approximate) Riemann solvers which are essential for the high-resolution upwind scheme. This advantage is especially important in the multi-dimensional case where there is no exact Riemann solver. Moreover, the central schemes are "genuinely multi-dimensional" in the sense that it does not necessitate dimensional spliting. Apart from these central scheme do not produce spurious oscillations, such as carbuncle phenomena and odd-even decoupling which usually happens in the Godunov upwind schemes. The reason of this advantage is the presence of sufficient numerical dissipation in the central schemes. This this also the reason here in the multicomponent flow that we see allmost negligible or no oscillations at the gases interface, for further details on numerical dissipation see Xu [37].

The organization of this paper is as follows:

In Section 2, we derive the three-dimensional Euler equations for the relativistic multi-component flows. We then discuss how to obtain the premitive variables from the conserved variables.

In Section 3 we write the one dimensional relativistic Euler equations for the dynamics of a mixture of two gases. Starting from the first order central scheme, we explain the

high-resolution second order central schemes to solve these Euler equations, see [24] and references therein.

In Section 4 we explain the scheme for the two-dimensional relativistic multi-component flows. We again start from the first order central schemes and then extend it to second order, see [13] and references therein.

In Section 5 we present numerical test cases which include, propagation of 1D relativistic blast waves, collision of two relativistic blast waves, cylinderical explosion, interaction of an air shock with helium bubble and explosion in a square box.

2 Multicomponent Relativistic Euler Equations

For simplicity we assume a model of mixture of two gases. The extension to more components is analogous. Let $\rho = \rho_1 + \rho_2$ denote the total density of the mixture, with ρ_1 and ρ_2 as the mass densities of the first and second components respectively. Also let Y_1 and Y_2 be the mass fractions of the first and second components.

We assume that both components are in thermal equilibrium and are perfect gases with specific heats at constant volume C_{v1}, C_{v2}, specific heats at constant pressure C_{p1}, C_{p2} and ratios of specific heats γ_1, γ_2. By standard thermodynamic arguments, the ratio of specific heats γ of the mixture of gases is

$$\gamma = \frac{C_p}{C_v} = \frac{Y_1 C_{p1} + Y_2 C_{p2}}{Y_1 C_{v1} + Y_2 C_{v2}} \,. \tag{1}$$

Using the Einstein summation convention the equations discribing the motion of a two-component relativistic fluid are given by the six conservation laws

$$\left(\rho_1 u^\mu\right)_{;\mu} = 0 \,, \qquad \left(\rho_2 u^\mu\right)_{;\mu} = 0 \,, \quad \left(T^{\mu\nu}\right)_{;\nu} = 0 \,, \tag{2}$$

where $(\mu, \nu = 0, ..., 3)$, and where $;\mu$ denote the covariant derivative with respect to coordinate x^μ. Furthermore, u^μ is the four-velocity of the mixture, and $T^{\mu\nu}$ is the stress-energy tensor, which for a perfect fluid can be written as

$$T^{\mu\nu} = \rho h u^\mu u^\nu + p g^{\mu\nu} \,. \tag{3}$$

Here $g^{\mu\nu}$ is metric tensor

$$g_{\mu\nu} = g^{\mu\nu} = \begin{cases} -1, & \mu = \nu = 0 \,, \\ 1, & \mu = \nu = 1, 2, 3 \,, \\ 0, & \mu \neq \nu \,, \end{cases}$$

ρ is the mixture density, p the fluid average pressure, and h the specific enthalpy of the fluid mixture defined by

$$h = 1 + \epsilon + \frac{p}{\rho}\,, \tag{4}$$

where ϵ is the specific internal energy. Note that we use natural units (i.e., the speed of light $c = 1$) through out this study. In Minskowski space time and cartesion coordinates (t, x^1, x^2, x^3), the conservation equations (2) can be written as

$$\frac{\partial w}{\partial t} + \frac{\partial f^i(w)}{\partial x^i} = 0\,, \tag{5}$$

with the conserved variables w and fluxes f^i given as

$$w = \begin{pmatrix} D_1 \\ D_2 \\ S^1 \\ S^2 \\ S^2\ \tau \end{pmatrix}\,, \qquad f^i = \begin{pmatrix} D_1 v^i \\ D_2 v^i \\ S^1 v^i + p\delta^{1i} \\ S^2 v^i + p\delta^{2i} \\ S^3 v^i + p\delta^{3i} \\ S^i - D v^i \end{pmatrix}\,. \tag{6}$$

The six conserved quantitites D_1, D_2, S^1, S^2, S^3 and τ are the rest-mass densities of the two components, the three components of momentum density, and the energy density (measured relative to the rest mass density), respectively. They are all measured in laboratory frame, and are related to quantities in the local rest frame of the fluid (primitive variables) through the relations

$$D_1 = \rho_2\Gamma\,, \quad D_2 = \rho_1\Gamma\,, \quad S^i = \rho h\Gamma^2 v^i\,, \quad \tau = \rho h\Gamma^2 - p - D\,, \tag{7}$$

where v^i are the components of three-velocity of fluid

$$v^i = \frac{u^i}{u^0}\,, \qquad i = 1, 2, 3,$$

with the lorentz factor $u^0 = \sqrt{1 + \mathbf{u}^2}$. Let us define Γ as

$$\Gamma = \frac{1}{\sqrt{1 - v^i v_i}}\,. \tag{8}$$

Note that $u^0 = \Gamma$, because $\mathbf{u} = \mathbf{v}/\sqrt{1 - \mathbf{v}^2}$. The system of equations (2) with definitions (5)-(8) is closed by mean of an ideal equation of state (EOS) as given below

$$p = (\gamma - 1)\rho\epsilon\,. \tag{9}$$

We denote by c_s the sound speed, defined by

$$hc_s^2 = \left.\frac{\partial p}{\partial \rho}\right|_s\,, \tag{10}$$

where s is the specific entropy, which is conserved along fluid lines. For EOS under consideration the speed of sound can be written as

$$c_s = \left(\frac{\gamma p}{\rho h}\right)^{\frac{1}{2}} . \tag{11}$$

The Mach number of the flow is due to Königl [17]

$$M = \frac{v}{c_s}\frac{\Gamma}{\Gamma_s} .$$

For any given initial macroscopic variables in space and time,

$$w_1 = \left(\rho_1, v_1^i, p_1\right) , \quad w_2 = \left(\rho_2, v_2^i, p_2\right) , \quad i = 1, 2, 3, \tag{12}$$

the common values of density ρ, velocity v^i, and pressure p can be obtained from the conservation requirements,

$$\begin{aligned} D &= (\rho_1\Gamma_1) + (\rho_2\Gamma_2) , \\ S^i &= \left(\rho_1 h_1 \Gamma_1^2 v_1^i\right) + \left(\rho_2 h_2 \Gamma_2^2 v_2^i\right) , \qquad i = 1, 2, 3, \\ \tau &= \left(\rho h_1 \Gamma_1^2 - p_1 - \rho_1\Gamma_1\right) + \left(\rho_1 h_1 \Gamma_2^2 - p_2 - \rho_2\Gamma_2\right) . \end{aligned} \tag{13}$$

From the above equations p, ρ and v^i can be obtained by first solving an implicit function of pressure whose zero represents the pressure, see Martí and E. Müller [23], as well as Aloy et al. [1]. We have to find the root of the equation

$$\eta(p) = (\gamma - 1)\,\rho_*\epsilon_* - p\,, \tag{14}$$

with ρ_* and ϵ_* given by

$$\rho_* = \frac{D}{\Gamma_*}, \quad \epsilon_* = \frac{\tau + D\,(1 - \Gamma_*) + p\,(1 - \Gamma_*^2)}{D\Gamma_*}\,, \tag{15}$$

where

$$\Gamma_* = \frac{1}{\sqrt{1 - \mathbf{v}_*^2}}\,, \quad \mathbf{v}_* = \frac{\mathbf{S}}{\tau + D + p}\,. \tag{16}$$

The monotonicity of $\eta(p) \in [p_{min}, \infty]$ ensures the uniqueness of the solution. The lower bound of the physically allowed domain, p_{min}, defined by

$$p_{min} = |\mathbf{S}| - \tau - D\,,$$

is obtained from $(7)_3$ by taking in to account that (in our units) $|\mathbf{v}| \leq 1$. Knowing p, $(16)_2$ then directly gives $\mathbf{v}$, while the density can be obtained from $(15)_1$ and $(16)_1$.

Similar to Aloy et al. [1], we obtained the solution $\eta(p) = 0$ by means of Newton-Rahphson iteration in which the derivative of η, i.e. η', is aopproximated by

$$\eta' = |\mathbf{v}_*|^2 c_{s*}^2 - 1\,, \tag{17}$$

wheree c_{s*} is the speed of sound given by

$$c_{s*} = \sqrt{\frac{(\gamma-1)\gamma\epsilon_*}{1+\gamma\epsilon_*}}, \tag{18}$$

This approximation tends to the exact derivative when the solution is approached. On the other hand, it easily allows one to extend the present algorithm to general equation of state, see [1].

3 One-dimensional Multicomponent Flows

Here we are looking for a spatially one-dimensional solutions of Euler equations. We only consider the solutions which depend on t and $x = x^1$ and satisy $\rho = \rho(t,x)$, $\rho_1 = \rho_1(t,x)$, $\rho_2 = \rho_2(t,x)$, $v = (v(t,x), 0, 0)$ and $p = p(t,x)$. The three dimensional Euler equations (5) then reduces to

$$\frac{\partial w}{\partial t} + \frac{\partial f(w)}{\partial x} = 0\,, \tag{19}$$

with the conserved variables w and fluxes f given as

$$w = \begin{pmatrix} D_1 \\ D_2 \\ S \\ \tau \end{pmatrix}\,, \qquad f = \begin{pmatrix} D_1 v \\ D_2 v \\ Sv + p \\ S - Dv \end{pmatrix}\,, \tag{20}$$

where

$$D_1 = \rho_1\Gamma\,, \quad D_2 = \rho_1\Gamma\,, \quad S = \rho h\Gamma^2 v\,, \quad \tau = \rho h\Gamma^2 - p - D\,, \tag{21}$$

and

$$v = \frac{u}{u^0}\,, \quad \Gamma = \frac{1}{\sqrt{1-v^2}}\,, \quad p = (\gamma-1)\rho\epsilon\,, \tag{22}$$

where $u^0 = \sqrt{1+u^2}$. For any given initial macroscopic variables in space and time,

$$w_1 = (\rho_1, v_1, p_1)\,, \quad w_2 = (\rho_2, v_2, p_2)\,, \tag{23}$$

the common values of density ρ, velocity v, and pressure p can be obtained from the conservation requirements,

$$\begin{aligned} D &= (\rho_1\Gamma_1) + (\rho_2\Gamma_2)\,, \\ S^i &= \left(\rho_1 h_1 \Gamma_1^2 v_1\right) + \left(\rho_2 h_2 \Gamma_2^2 v_2\right)\,, \\ \tau &= \left(\rho h_1 \Gamma_1^2 - p_1 - \rho_1\Gamma_1\right) + \left(\rho_1 h_1 \Gamma_2^2 - p_2 - \rho_2\Gamma_2\right)\,. \end{aligned} \tag{24}$$

From the above equations p, ρ, and v can be obtained by following the same procedure as given in relations (14) to (18).

3.1 One-Dimensional Central Schemes

Let us begin by introducing the well-known first order Lax-Friedrichs (LxF) scheme for one-dimensional conservation laws. This first order scheme is then extended to a second order central scheme, see [24]. We consider a piecewise-constant initial data, $\sum \overline{w}_i^n \chi_i(x)$, where, $\chi_i(x)$ is a characteristic function of the cell, $I_i := \{\xi \mid |\xi - x_i| \leq \frac{\Delta x}{2}\}$, centered arround $x_i = i\Delta x$. Integrating (19) over the rectangle $[x_i, x_{i+1}] \times [t^n, t^{n+1}]$, we get

$$\oint_{\partial\Omega} w dx - f(w)dt = 0 \Leftrightarrow$$

$$-\int_{t^n}^{t^{n+1}} f\left(w(t, x_i)\right) dt + \int_{x_i}^{x_{i+1}} w(t^{n+1}, \xi)d\xi + \int_{t^n}^{t^{n+1}} f\left(w(t, x_{i+1})\right) dt - \int_{x_i}^{x_{i+1}} w(t^n, \xi)d\xi = 0\,.$$

Note that our cells I_i are staggered with respect to the interval $[x_i, x_{i+1}]$ of integration. This leads to the LxF scheme

$$\overline{w}_{i+\frac{1}{2}}^{n+1} = \frac{1}{2}(\overline{w}_i^n + \overline{w}_{i+1}^n) + \lambda\left(f(w_i^n) - f(w_{i+1}^n)\right)\,, \quad w_i^n := w(t^n, x_i) = \overline{w}_i^n\,, \tag{25}$$

where $\lambda = \frac{\Delta t}{\Delta x}$. The piecewise constant cells in each step are staggered with respect to those in the previous step.

Extension to Higher Order:

Starting with a piecewise-constant solution in time and space, $\sum \overline{w}_i^n \chi_i(x)$, one reconstruct a piecewise linear (MUSCL-type) approximation in space, namely

$$w(t^n, x) = \sum \left(\overline{w}_i^n + w_i^x \frac{(x - x_i)}{\Delta x}\right) \chi_i(x)\,, \tag{26}$$

where w_i^x abbreviates a first-order discrete slopes, see Figure 1. A possible computation of these slopes, which results in an overall nonoscillatory scheme (consult [24]), is given by family of *discrete derivatives* parameterized with $1 \leq \theta \leq 2$, i.e., for any grid function $\{w_i\}$ we set

$$w_i^x = MM\theta\{w_{i-1}, w_i, w_{i+1}\} = MM\left(\theta\Delta w_{i+\frac{1}{2}}, \frac{\theta}{2}(\Delta w_{i-\frac{1}{2}} + \Delta w_{i+\frac{1}{2}}), \theta\Delta w_{i-\frac{1}{2}}\right) \tag{27}$$

Here, Δ denotes the central differencing, $\Delta w_{i+\frac{1}{2}} = w_{i+1} - w_i$, and MM denotes the min-mod nonlinear limiter

$$MM\{x_1, x_2, ...\} = \begin{cases} \min_i\{x_i\} & \text{if } x_i > 0 \quad \forall i\,, \\ \max_i\{x_i\} & \text{if } x_i < 0 \quad \forall i\,, \\ 0 & \text{otherwise}\,. \end{cases} \tag{28}$$

This interpolant, (26), is then evolved exactly in time and projected on the staggered cell-averages on the next time step, t^{n+1}. Consider the balance law over the control volume

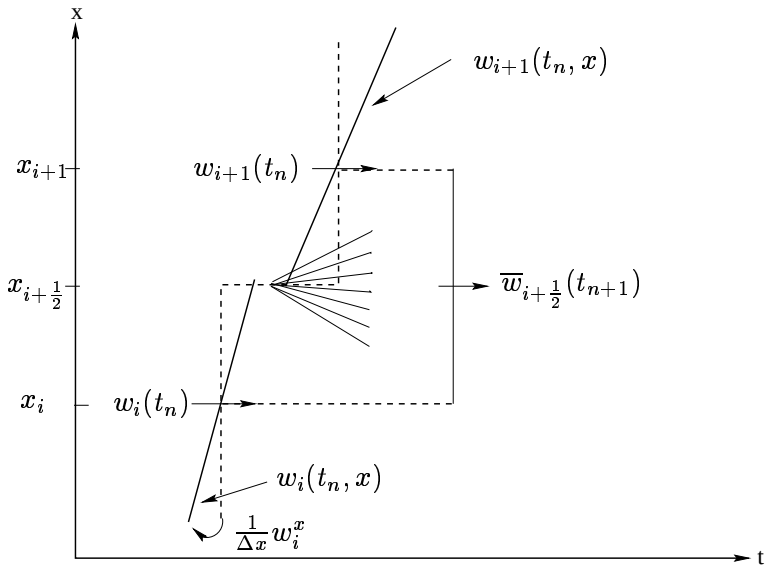

Figure 1: Second Order Reconstruction

$[x_{i-\frac{1}{2}}, x_{i+\frac{1}{2}}] \times [t^n, t^{n+1}]$, we have

$$\oint_{\partial\Omega} w dx - f(w) dt = 0 \Leftrightarrow$$

$$-\int_{t^n}^{t^{n+1}} f(w_i(t)) dt + \int_{x_i}^{x_{i+1}} w(t^{n+1}, \xi) d\xi + \int_{t^n}^{t^{n+1}} f(w_{i+1}(t)) dt - \int_{x_i}^{x_{i+1}} w(t^n, \xi) d\xi = 0 \,.$$

This yields

$$\overline{w}_{i+\frac{1}{2}}^{n+1} = \overline{w}_{i+\frac{1}{2}}(t^n) + \lambda \left(\frac{1}{\Delta t} \int_{t^n}^{t^{n+1}} f(w_i(\tau)) d\tau - \frac{1}{\Delta t} \int_{t^n}^{t^{n+1}} f(w_{i+1}(\tau)) d\tau \right) \,. \tag{29}$$

Where $\lambda = \frac{\Delta t}{\Delta x}$. The averaging of the linear data (26) at $t = t^n$, yields

$$\begin{aligned} \overline{w}_{i+\frac{1}{2}}^n &= \frac{1}{\Delta x} \int_{x_i}^{x_{i+1}} w(t^n, \xi) d\xi \\ &= \frac{1}{\Delta x} \left(\int_{x_i}^{x_{i+\frac{1}{2}}} w_i(t^n, \xi) d\xi + \int_{x_{i+\frac{1}{2}}}^{x_{i+1}} w_{i+1}(t^n, \xi) d\xi \right) \,, \\ &= \frac{1}{2}(w_i^n + w_{i+1}^n) + \frac{1}{8}(w_i^x - w_{i+1}^x) \,. \end{aligned} \tag{30}$$

So far every thing is *exact*. Moreover the Courant-Friedrichs-Levy (CFL) condition guarantees that $f(w_i(\tau))$ and $f(w_{i+1}(\tau))$, are smooth functions of τ; hence they can be integrated approximatly by the mid point rule at the expense of an $O(\Delta t)^3$ local truncation error. Thus we can write

$$\frac{1}{\Delta t}\int_{t^n}^{t^{n+1}} f(w_{i+1}(t))dt \sim f(w_i(t^{n+\frac{1}{2}})) + O(\Delta t)^3 \,. \tag{31}$$

Putting (30) and (31) in (29) we finally get

$$\overline{w}_{i+\frac{1}{2}}^{n+1} = \frac{1}{2}(w_i^n + w_{i+1}^n) + \frac{1}{8}(w_i^x - w_{i+1}^x) + \lambda\left[f(w_i(t^{n+\frac{1}{2}})) - f(w_{i+1}(t^{n+\frac{1}{2}}))\right] . \tag{32}$$

By Taylor expansion and the conservation laws (19), we have

$$w_i^{n+\frac{1}{2}} = w_i(t^{n+\frac{1}{2}}) = \overline{w}_i^n + \frac{\Delta t}{2}(w_i)_t(t^n) + O(\Delta t)^2 = \overline{w}_i^n - \frac{\lambda}{2}f^x(w_i) + O(\Delta t)^2 \,. \tag{33}$$

This may serve as our approximate midvalues $w_i^{n+\frac{1}{2}}$ within the permissible second-order accuracy requirement. Here, $\frac{1}{\Delta x}f^x(w_i)$ stands for an approximate numerical derivatives of the flux $f(w(t, x = x_i))$,

$$\frac{1}{\Delta x}f^x(w_i) = \frac{\partial}{\partial x}f(w(t, x = x_i) + O(\Delta x)$$

The fluxes $f^x(w_i)$ are computed by applying the min-mod limiter to each of the component of f, i.e.,

$$\begin{aligned} F^x(w_i) &= MM\theta\{F(w_{i-1}), F(w_i), F(w_{i+1})\} \\ &= MM\left(\theta\Delta F(w_{i+\frac{1}{2}}), \frac{\theta}{2}\left(\Delta F(w_{i-\frac{1}{2}}) + \Delta F(w_{i+\frac{1}{2}})\right), \theta\Delta F(w_{i-\frac{1}{2}})\right) . \end{aligned}$$

Here, Δ denotes the central differencing, $\Delta F(w_{i+\frac{1}{2}}) = F(w_{i+1}) - F(w_i)$, and MM denotes the min-mod nonlinear limiter given by (28).

This componentwise approach is one of the main advantages offered by central schemes over corresponding characteristic decompositions required by upwind schemes, see [13] and [24]. It is important to emphasize that while using the central type LxF solver, we integrate over the entire Riemann fan, which consists of both the left and rightgoing waves. On the one hand, this enables us to ignore the detailed knowledge about the exact (or approximate) generalized Riemann solver. On the other hand, this enable us to accurately compute the numerical flux $\int_{t_n}^{t_{n+1}} f(w(\tau, x))d\tau$, whose values are extracted from the smooth interface of two non-interacting Riemann problems.

In summary, this family of central differencing scheme takes the easily implemented predictor-corrector form,

$$w_i^{n+\frac{1}{2}} = \overline{w}_i^n - \frac{\lambda}{2} f^x(w_i)\,, \tag{34}$$

$$\begin{aligned}\overline{w}_{i+\frac{1}{2}}^{n+1} =& \frac{1}{2}(\overline{w}_i^n + \overline{w}_{i+1}^n) + \frac{1}{8}(w_i^x - w_{i+1}^x) \\ &+ \lambda\left[f(w_i(t^{n+\frac{1}{2}})) - f(w_{i+1}(t^{n+\frac{1}{2}}))\right]\,.\end{aligned} \tag{35}$$

4 Two-Dimensional Multicomponent Flows

Here we are looking for a spatially two-dimensional solutions of the multicomponent Euler equations. We only consider the solutions which depend on t, $x = x^1$, $y = x^2$ and satisfy $\rho = \rho(t,x,y)$, $\rho_1 = \rho_1(t,x,y)$, $\rho_2 = \rho_2(t,x,y)$, $\mathbf{v} = (v_1(t,x), v_2(t,y), 0)$ and $p = p(t,x,y)$. The three dimensional Euler equations (5) then reduces to

$$\frac{\partial w}{\partial t} + \frac{\partial f(w)}{\partial x} + \frac{\partial g(w)}{\partial y} = 0\,, \tag{36}$$

the conserved variables w and fluxes f, g are given by

$$w = \begin{pmatrix} D_1 \\ D_2 \\ S^1 \\ S^2 \\ \tau \end{pmatrix}\,, \quad f = \begin{pmatrix} D_1 v^1 \\ D_2 v_1 \\ S^1 v_1 + p \\ S^2 v_1 \\ S^1 - D v_1 \end{pmatrix}\,, \quad g = \begin{pmatrix} D_1 v_2 \\ D_2 v_2 \\ S^1 v_2 \\ S^2 v_2 + p \\ S^2 - D v_2 \end{pmatrix}\,, \tag{37}$$

where

$$D_1 = \rho_1\Gamma\,, \quad D_2 = \rho_2\Gamma\,, \quad S^1 = \rho h \Gamma^2 v_1\,, \quad S^2 = \rho h \Gamma^2 v_2\,, \quad \tau = \rho h \Gamma^2 - p - D\,, \tag{38}$$

and

$$v_1 = \frac{u^1}{u^0}\,, \quad v_2 = \frac{u^2}{u^0}\,, \quad \Gamma = \frac{1}{\sqrt{1-(v_1^2+v_2^2)}}\,, \quad p = (\gamma-1)\rho\epsilon\,. \tag{39}$$

where $u^0 = \sqrt{1+u_1^2+u_2^2}$. For any given initial macroscopic variables in space and time,

$$w_1 = \left(\rho_1, v_1^i, p_1\right)\,, \quad w_2 = \left(\rho_2, v_2^i, p_2\right)\,, \quad i = 1,2, \tag{40}$$

the common values of density ρ, velocity v^i, and pressure p can be obtained from the conservation requirements,

$$\begin{aligned} D &= (\rho_1\Gamma_1) + (\rho_2\Gamma_2)\,, \\ S^i &= \left(\rho_1 h_1 \Gamma_1^2 v_1^i\right) + \left(\rho_2 h_2 \Gamma_2^2 v_2^i\right)\,, \qquad i = 1,2, \\ \tau &= \left(\rho h_1 \Gamma_1^2 - p_1 - \rho_1\Gamma_1\right) + \left(\rho_1 h_1 \Gamma_2^2 - p_2 - \rho_2\Gamma_2\right)\,. \end{aligned} \tag{41}$$

From the above equations p, ρ and v^i can be obtained by follwing the same procedure as given in relations (14) to (18) for this spatially two-dimensional case.

4.1 Two-Dimensional Central Schemes

To approximate (36), we begin with a piecewise constant solution of the form $\sum \overline{w}^n_{i,j}\chi_{i,j}(x,y)$. We denote by $\overline{w}^n_{i,j}$, the approximate cell-average at time $t = t^n$, associated with the cell $C_{i,j} = I_i \times J_j$, centered arround $(x_i = i\Delta x,\, y_j = j\Delta y)$, i.e.,

$$C_{i,j} = \left\{ (\xi,\eta) \;\middle|\; |\xi - x_i| \le \frac{\Delta x}{2},\ |\xi - y_j| \le \frac{\Delta y}{2} \right\},$$

and $\chi_{i,j}(x,y)$ is a characteristic function of the cell $C_{i,j}$.

The arguments applied to the one-dimensional case can be easily extended to the higher dimensions. In the following we will abbreviate $\fint_B = \frac{1}{|B|}\int_B$ to denote the normalized integral, i.e., normalized over its length, area, etc. Also let $\lambda = \frac{\Delta t}{\Delta x}$ and $\mu = \frac{\Delta t}{\Delta y}$ denote the fixed mesh-ratio in the x- and y-directions, respectively. Let

$$\overline{w}_{i+\frac{1}{2},j+\frac{1}{2}}(t) = \fint_{C_{i+\frac{1}{2},j+\frac{1}{2}}} w(t,x,y)dxdy$$

denote the staggered averages. Integrating (36) over the volume $[i,i+1]\times[j,j+1]\times[t^n,t^{n+1}]$, we get,

$$\begin{aligned}
\overline{w}^{n+1}_{i+\frac{1}{2},j+\frac{1}{2}} = &\fint_{C_{i+\frac{1}{2},j+\frac{1}{2}}} w(t^n,x,y)dxdy \\
&- \lambda\left\{ \fint_{t^n}^{t^{n+1}} \fint_{y_j}^{y_{j+1}} \left[f(w(t,x_{i+1},y)) - f(w(t,x_i,y))\right] dydt \right\} \\
&- \mu\left\{ \fint_{t^n}^{t^{n+1}} \fint_{x_i}^{x_{i+1}} \left[g(w(t,x,y_{j+1})) - g(w(t,x,y_j))\right] dxdt \right\}
\end{aligned}$$

As given in Figure 2, the first integral has contribution from the four cells $C_{i,j}$, $C_{i+1,j}C_{i+1,j+1}$, and $C_{i,j+1}$. Simplifying the above balance law we finally get the following LxF scheme,

$$\begin{aligned}
\overline{w}^{n+1}_{i+\frac{1}{2},j+\frac{1}{2}} = &\frac{1}{4}(\overline{w}^n_{i,j} + \overline{w}^n_{i+1,j} + \overline{w}^n_{i,j+1} + \overline{w}^n_{i+1,j+1}) \\
&- \frac{\lambda}{2}\left(f(w^n_{i+1,j}) - f(w^n_{i,j}) + f(w^n_{i+1,j+1}) - f(w^n_{i,j+1})\right) \\
&- \frac{\mu}{2}\left(g(w^n_{i,j+1}) - g(w^n_{i,j}) + g(w^n_{i+1,j+1}) - g(w^n_{i+1,j})\right) \qquad (42)
\end{aligned}$$

A Second-Order Extension in 2D:

A two-dimensional extension of the second order central scheme was introduced in [13]. As in one-dimensional case, this staggered scheme can be viewed as an extension to the

first-order LxF Scheme. A piecewise-linear interpolant is reconstructed from the calculated cell-averages at time t^n,

$$w(t^n,x,y)=\sum\left(\overline{w}^n_{i,j}+w^x_{i,j}\left(\frac{x-x_i}{\Delta x}\right)+w^y_{i,j}\left(\frac{y-y_j}{\Delta y}\right)\right)\chi_{i,j}(x,y)\,. \tag{43}$$

Here $w^x_{i,j}$ and $w^y_{i,j}$ are discrete slopes in the $x-$ and $y-$directions, respectively, which are reconstructed from the given cell averages. To guarantee second-order accuracy, these slopes should approximate the corresponding derivatives,

$$w^x_{i,j}\sim\Delta x\frac{\partial}{\partial x}w(t^n,x_i,y_j)+O(\Delta x)^2\,,\qquad w^y_{i,j}\sim\Delta y\frac{\partial}{\partial x}w(t^n,x_i,y_j)+O(\Delta y)^2\,. \tag{44}$$

A possible computation of these slopes, which results in an overall nonoscillatory schemes is given by family of *discrete derivatives* parameterized with $1\le\theta\le 2$, for example

$$w^x_{i,j}=MM\left\{\theta(\overline{w}^n_{i+1,j}-\overline{w}^n_{i,j}),\frac{\theta}{2}(\overline{w}^n_{i+1,j}-\overline{w}^n_{i-1,j}),\theta(\overline{w}^n_{i,j}-\overline{w}^n_{i-1,j})\right\}\,, \tag{45}$$

$$w^y_{i,j}=MM\left\{\theta(\overline{w}^n_{i,j+1}-\overline{w}^n_{i,j}),\frac{\theta}{2}(\overline{w}^n_{i,j+1}-\overline{w}^n_{i,j-1}),\theta(\overline{w}^n_{i,j}-\overline{w}^n_{i,j-1})\right\}\,. \tag{46}$$

Here MM denotes the min-mod nonlinear limiter given by (28). This guarantees that the corresponding piecewise-linear reconstruction in (43), $w(t^n,x,y)$, is co-monotone with the underlying piecewise-constant approximation, $\sum\overline{w}^n_{i,j}\chi_{i,j}(x,y)$.

Similar to one-dimensional case, the construction of the central scheme proceeds with a second step of an exact evolution. The integration of (36) over volume $[i,i+1]\times[j,j+1]\times[t^n,t^{n+1}]$ yields

$$\begin{aligned}\overline{w}^{n+1}_{i+\frac12,j+\frac12}=&\fint_{C_{i+\frac12,j+\frac12}}w(t^n,x,y)dxdy\\&-\lambda\left\{\fint_{t^n}^{t^{n+1}}\int_{y_j}^{y_{j+1}}[f(w(t,x_{i+1},y))-f(w(t,x_i,y))]dydt\right\}\\&-\mu\left\{\fint_{t^n}^{t^{n+1}}\int_{x_i}^{x_{i+1}}[g(w(t,x,y_{j+1}))-g(w(t,x,y_j))]dxdt\right\}\,.\end{aligned} \tag{47}$$

We begin by evaluating the cell average $\fint_{C_{i+\frac12,j+\frac12}}w(t^n,x,y)dxdy$. As before it has contribution from the four intersecting cells, $C_{i,j}$, $C_{i+1,j}$, $C_{i+1,j+1}$, and $C_{i,j+1}$. Starting with the intersecting cell $C_{i,j}$ at the corner (see Figure 2), $C^{SW}_{i+\frac12,j+\frac12}=C_{i+\frac12,j+\frac12}\cap C_{i,j}$, we find the average of the reconstructed polynomial in (43),

$$\begin{aligned}\fint_{C^{SW}_{i+\frac12,j+\frac12}}w(t^n,x,y)dxdy&=\int_{x_i}^{x_{i+\frac12}}\int_{y_j}^{y_{j+\frac12}}\left(\overline{w}^n_{i,j}+w^x_{i,j}\left(\frac{x-x_i}{\Delta x}\right)+w^y_{i,j}\left(\frac{y-y_i}{\Delta y}\right)\right)dxdy\\&=\frac14\overline{w}^n_{i,j}+\frac{1}{16}(w^x_{i,j}+w^y_{i,j})\,.\end{aligned} \tag{48}$$

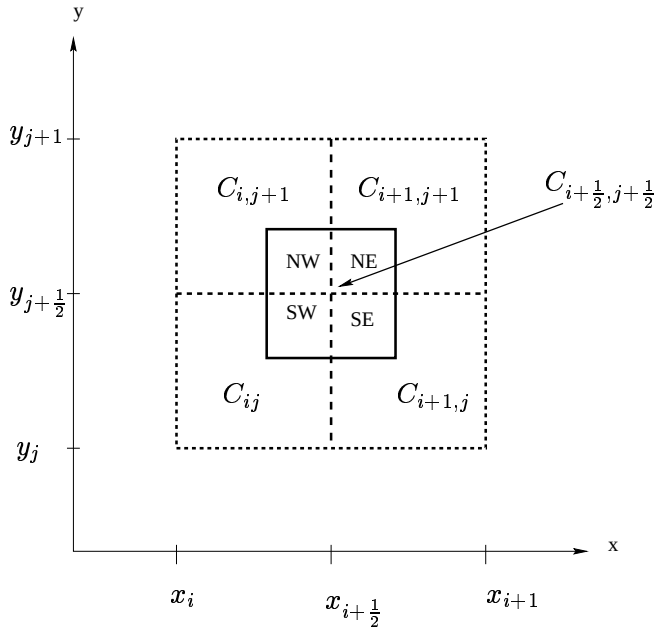

Figure 2: Floor plane of the staggered grid.

Continuing in a counter clockwise direction, we have

$$\oint_{C^{SE}_{i+\frac{1}{2},j+\frac{1}{2}}} w(t^n,x,y)dxdy = \frac{1}{4}\overline{w}^n_{i+1,j} + \frac{1}{16}(-w^x_{i+1,j} + w^y_{i+1,j})\,, \tag{49}$$

$$\oint_{C^{NE}_{i+\frac{1}{2},j+\frac{1}{2}}} w(t^n,x,y)dxdy = \frac{1}{4}\overline{w}^n_{i+1,j+1} - \frac{1}{16}(w^x_{i+1,j+1} + w^y_{i+1,j+1})\,, \tag{50}$$

$$\oint_{C^{NW}_{i+\frac{1}{2},j+\frac{1}{2}}} w(t^n,x,y)dxdy = \frac{1}{4}\overline{w}^n_{i,j+1} + \frac{1}{16}(w^x_{i,j+1} - w^y_{i,j+1})\,. \tag{51}$$

By adding the last four integrals we find that the exact staggered averages of the reconstructed solution at $t = t^n$.

$$\begin{aligned}\overline{w}^n_{i+\frac{1}{2},j+\frac{1}{2}} =& \oint_{C_{i+\frac{1}{2},j+\frac{1}{2}}} w(t^n,x,y)dxdy \\ =& \frac{1}{4}\left(\overline{w}^n_{i,j} + \overline{w}^n_{i+1,j} + \overline{w}^n_{i,j+1} + \overline{w}^n_{i+1,j+1}\right) \\ &+ \frac{1}{16}\{(w^x_{i,j} - w^x_{i+1,j}) + (w^x_{i,j+1} - w^x_{i+1,j+1}) \\ &+ (w^y_{i,j} - w^y_{i,j+1}) + (w^y_{i+1,j} - w^y_{i+1,j+1})\}\,. \end{aligned} \tag{52}$$

So far every thing is *exact*. We now turn to *approximating* the four fluxes on the right of (47), starting with the one along the east face (consult Figure 3), i.e.

$$\oint_{t^n}^{t^{n+1}} \oint_{y\in J_{j+\frac{1}{2}}} f(w(t,x_{i+1},y))dydt.$$

We use midpoint quadrature rule for second-order approximation of the temporal integral ,

$$\oint_{y\in J_{j+\frac{1}{2}}} f(w(t^{n+\frac{1}{2}}, x_{i+1}, y))dy\,,$$

and, for the reasons to be clarified below, we use the second-order rectangular quadrature rule for the spatial integration across the y-axis, yielding

$$\oint_{t^n}^{t^{n+1}} \oint_{y\in J_{j+\frac{1}{2}}} f(w(t, x_{i+1}, y))dydt \sim \frac{1}{2}\left(f(w_{i+1,j}^{n+\frac{1}{2}}) + f(w_{i+1,j+1}^{n+\frac{1}{2}})\right)\,. \tag{53}$$

In similar manner we approximate the remaining fluxes,

$$\oint_{t^n}^{t^{n+1}} \oint_{x\in I_{i+\frac{1}{2}}} g(w(t, x, y_{j+1}))dxdt \sim \frac{1}{2}\left(g(w_{i,j+1}^{n+\frac{1}{2}}) + gw_{i+1,j+1}^{n+\frac{1}{2}})\right)\,, \tag{54}$$

$$\oint_{t^n}^{t^{n+1}} \oint_{y\in J_{j+\frac{1}{2}}} f(w(t, x_i, y))dydt \sim \frac{1}{2}\left(f(w_{i,j}^{n+\frac{1}{2}}) + f(w_{i,j+1}^{n+\frac{1}{2}})\right)\,, \tag{55}$$

$$\oint_{t^n}^{t^{n+1}} \oint_{x\in I_{i+\frac{1}{2}}} g(w(t, x, y_j))dxdt \sim \frac{1}{2}\left(g(w_{i,j}^{n+\frac{1}{2}}) + g(w_{i+1,j}^{n+\frac{1}{2}})\right)\,. \tag{56}$$

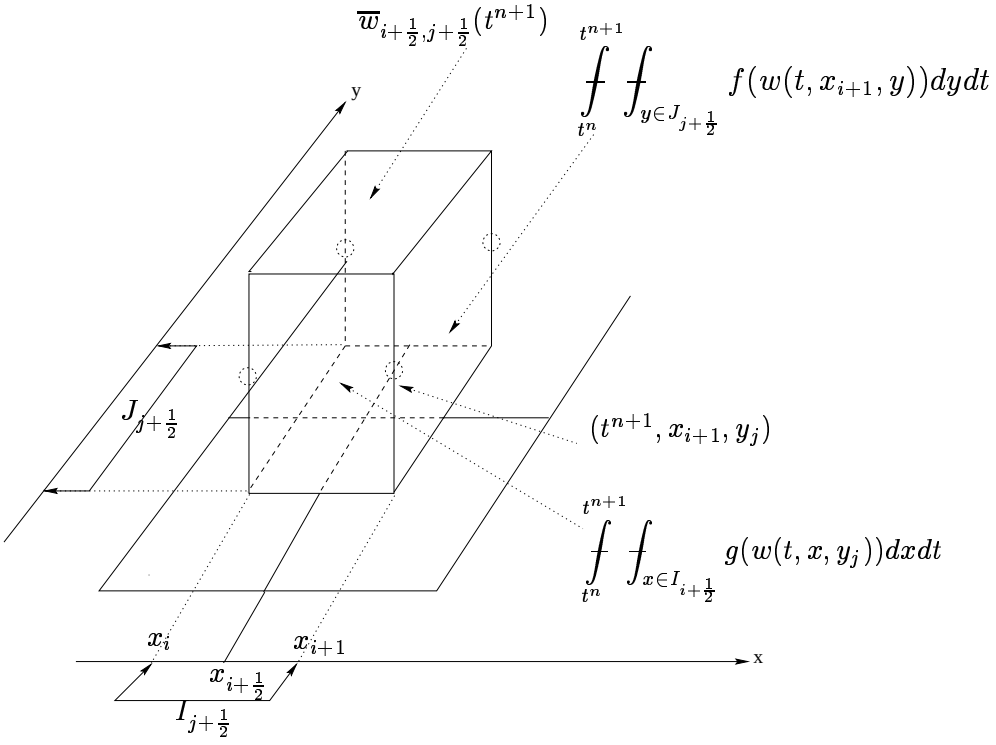

Figure 3: The central, staggered stencil.

The fluxes in (53)-(56) use the midpoint values, $w_{i,j}^{n+\frac{1}{2}} = w(t^{n+\frac{1}{2}}, x_i, y_j)$, and it is here that we take advantage of utilizing these midvalues for the spatial integration by the rectangular

rule. Namely, since these midvalues are secured at the smooth center of their cells, $C_{i,j}$, bounded away from the jump discontinuities along the edges, we may use Taylor expansion,

$$w(t^{n+\frac{1}{2}}, x_i, y_j) = \overline{w}^n_{i,j} + \frac{\Delta t}{2} w_t(t^n, x_i, y_j) + O(\Delta t)^2 .$$

Finally, we use the differential form of conservation laws (36) to express the time derivative, w_t, in term of the spatial derivatives, $f(w)_x$ and $g(w)_x$,

$$\begin{aligned} w^{n+\frac{1}{2}}_{i,j} &= \overline{w}^n_{i,j} - \frac{\Delta t}{2}\frac{\partial}{\partial x} f(w_{i,j}) - \frac{\Delta t}{2}\frac{\partial}{\partial y} g(w_{i,j}) + O(\Delta t)^2 \\ &= \overline{w}^n_{i,j} - \frac{\lambda}{2} f^x(w_{i,j}) - \frac{\mu}{2} g^y(w_{i,j}) + O(\Delta t)^2 . \end{aligned} \tag{57}$$

Here,

$$f^x(w_{i,j}) \sim \Delta x \frac{\partial}{\partial x} f(w(t^n, x_i, y_j)) + O(\Delta x)^2, \quad g^y(w_{i,j}) \sim \Delta y \frac{\partial}{\partial y} g(w(t^n, x_i, y_j)) + O(\Delta y)^2 ,$$

are one-dimensional discrete slopes of the fluxes in the x- and y-directions, of the type reconstructed in (44). We find these slopes in the same way as done for the conservative filed variables using min-mod procedure. Inserting these values, together with the staggered averages computed in (52), into (47), we conclude with new staggered averages at $t = t^{n+1}$, given by

$$\begin{aligned} \overline{w}^{n+1}_{i+\frac{1}{2},j+\frac{1}{2}} =& \frac{1}{4}(\overline{w}^n_{i,j} + \overline{w}^n_{i+1,j} + \overline{w}^n_{i,j+1} + \overline{w}^n_{i+1,j+1}) \\ &+ \frac{1}{16}(w^x_{i,j} - w^x_{i+1,j}) - \frac{\lambda}{2}\left(f(w^{n+\frac{1}{2}}_{i+1,j}) - f(w^{n+\frac{1}{2}}_{i,j})\right) \\ &+ \frac{1}{16}(w^x_{i,j+1} - w^x_{i+1,j+1}) - \frac{\lambda}{2}\left(f(w^{n+\frac{1}{2}}_{i+1,j+1}) - f(w^{n+\frac{1}{2}}_{i,j+1})\right) \\ &+ \frac{1}{16}(w^y_{i,j} - w^y_{i,j+1}) - \frac{\mu}{2}\left(g(w^{n+\frac{1}{2}}_{i,j+1}) - g(w^{n+\frac{1}{2}}_{i,j})\right) \\ &+ \frac{1}{16}(w^y_{i+1,j} - w^y_{i+1,j+1}) - \frac{\mu}{2}\left(g(w^{n+\frac{1}{2}}_{i+1,j+1}) - g(w^{n+\frac{1}{2}}_{i+1,j})\right) . \end{aligned} \tag{58}$$

In summary, we end up with a simple two-step predictor-corector scheme (57)-(58). Starting with the cell averages, $\overline{w}^n_{i,j}$, we use the first-order predictor (57) for the evolution of the midpoint values, $\overline{w}^{n+\frac{1}{2}}_{i,j}$, which is followed by the second-order corrector (58) for computation of the new cell averages, $\overline{w}^{n+1}_{i,j}$. This results in a second-order accurate nonoscillatory central schemes. As in the one-dimensional case no exact (approximate) Riemann solvers are involved. The nonoscillatory behaviour of the scheme hings on the reconstructed diecrete slopes, w^x,w^y, $f^x(w)$, and $g^y(w)$.

5 Numerical Test Cases

5.1 One-dimensional Test Problems

Here we present four one-domensional numerical probelms in order to validate the application of one-dimensional central schemes for the solution of one-dimensional multicomponent flow problems.

Problem 1: Propagation of relativistic blast waves:

$$\begin{aligned} W_l = (\rho_l, u_l, p_l, \gamma_l, C_{vl}) &= (10.0, 0.0, 13.33, 1.4, 1.0) \qquad \text{if } x < 0.5\,, \\ W_r = (\rho_r, u_r, p_r, \gamma_r, C_{vr}) &= (1.0, 0.0, 0.66 \times 10^{-6}, 1.67, 1.0) \quad \text{if } x \geq 0.5\,, \end{aligned}$$

where the computational domain is $0 \leq x \leq 1$ with 400 meh points. This test problem has been considered by several authors in one-component case, for example, Hawley, Smarr and Wilson [12], Schneider et al. [30], Martí and Müller [21, 23] etc. It involves the formation of an intermediate state bounded by a shock wave propagating to the right and transonic rarefaction wave propagating to the left. The fluid in the intermediate state moves at a mildly relativistic speed ($v = 0.7098c$) to the right. Flow particles accumulate in a dense shell behind the shock wave compressing the fluid by a factor of 5 and heating it up to values of internal energy much larger than the rest-mass energy. Hence the fluid is extremly relativistic in thermodynamical point of view, but mildly relativistic dynamically. The resutls are shown in Figure 5.

Problem 2: The initial data are:

$$\begin{aligned} W_l = (\rho_l, u_L, p_l, \gamma_l, C_{vl}) &= (1.0, 0.0, 1000.0, 1.4, 1.0) \qquad \text{if } x < 0.5\,, \\ W_r = (\rho_r, u_R, p_r, \gamma_r, C_{vr}) &= (1.0, 0.0, 0.01, 1.67, 1.0) \qquad \text{if } x \geq 0.5\,, \end{aligned}$$

where the computational domain is $0 \leq x \leq 1$ with 400 meh points. This problem was first considered in single-component case by Norman and Winkler [26]. The flow pattern is similar to that of problem 1, but more extreme. In case of 4000 mesh points the elativistic effects reduces the post-shock state to a thin dense shell with a width of only about 2% of the grid length at t=0.35. The fluid in the shell moves with $v_{\text{shell}} = 0.957$ (i.e., $\Gamma_{\text{shell}} = 3.35$), while jump in density in the shell reaches a value of 8.17. The resutls are shown in Figure 6.

Problem 3: Collision of two relativistic blast waves:

$$\begin{aligned} W_l = (\rho_l, u_L, p_l, \gamma_l, C_{vl}) &= (1.0, 0.0, 1000.0, 1.4, 1.0) \qquad \text{if } x <= 0.1\,, \\ W_m = (\rho_m, u_m, p_m, \gamma_m, C_{vm}) &= (1.0, 0.0, 0.01.0, 1.67, 1.0) \qquad \text{if } 0.1 < x < 0.9 \qquad , \\ W_r = (\rho_r, u_R, p_r, \gamma_r, C_{vr}) &= (1.0, 0.0, 100.0, 1.4, 1.0) \qquad \text{if } x \geq 0.9\,, \end{aligned}$$

where the computational domain is $0 \leq x \leq 1$. The collision of two strong blast waves was used by Woodward and Colella [35] to compare the performance of several numerical method in classical hydrodynamics. In the relativistic case, Yang et al. [38] considered this problem to test the high-order extensions of relativistic beam scheme, wherease Martí and Müller [21] used it to evaluate the performance of their relativistic PPM code. In this last case, the original boundary conditions were changed from (from reflecting to out flow) to avoid the reflection and subsequent interaction of rarefaction waves allowing for a comparison with an analytical solution. We will also consider the out flow boundary conditions in this example.

The initial data correspond to this test, consisting in three constant states with specific heat ratios jumps and large pressure jumps at the interfaces, which are located at $x = 0.1$ and $x = 0.9$. The propagation velocity of the two blast waves is slower than in the Newtonian case, but close to the speed of light (0.9644 and -0.881 for shock wave propagating to the right and left, respectively). Hence the shock interaction occurs much later (at t=0.43) than in the Newtonian problem (at about t=0.028). The collosion give rise to a narrow region of very high density bounded by two shocks.

Problem 4: A similar problem in non-relativistic case was solved by Quirk and Karni [27]. It consist of a $Ms = 1.14$ shock tube filled with air, where shock wave moves to the left. In the preshock wave stage, a bubble of Helium is set .The initial data are as follow

$$W = (\rho = 1.0,\, u = 0.0,\, p = 2.0,\, \gamma = 1.4,\, C_v = 0.72)\,, \text{pre-shoc air}$$
$$W = (\rho = 1.2977,\, u = -0.155947,\, p = 2.88387,\, \gamma = 1.4\,, C_v = 0.72)\,, \text{post-shoc air}$$
$$W = (\rho = 0.138,\, u = 0.0,\, p = 1.0,\, \gamma = 1.67,\, C_v = 2.42)\,, \text{helium}\,.$$

where the computational domain is $0 \leq x \leq 1$. We compute the approximate solution of this problem with a grid of 400 mesh points at time $t = 0.65$. For comparison purpose we use the same scheme with 3000 mesh points. The results are shown in Figure 8.

5.2 Two-dimensional Test Problems

Problem 5: Cylindrical Explosion Problem:

Consider a square domain $[0, 1] \times [0, 1]$. The initial data are constant in two regions separated by a circle of radius 0.2 centered at $(0.5, 0.5)$. Inside the circle is helium with density 10.0 and pressure 13.33, while outside is air of density 1.0 and pressure equal to 0.066×10^{-6}. The velocities are zero everywhere. The specific heat ratios for helium and air are 1.67 and 1.4, while specific heats at constant volume are equal to 1 for both air and helium. The solution consits of a circular shock wave propagating outwards from the origin, followed by a circular contact discontinuity propagating in the same direction, and a circular rarefaction wave travelling towards the origin. The results ar shown in Figure 9 for 400 mesh points at $t = 0.15$.

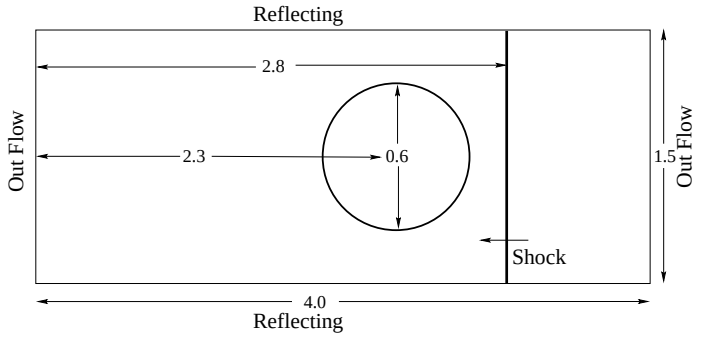

Figure 4: Sketch of computational domain .

Problem 6: A $Ms = 1.16$ shock wave in air hits a Helium cylinderical bubble:

In this example we introduce a single planar shock, moving in the air, with a cylinderical bubble of Helium. A schematic description of computational set-up is shown in Figure 4, where reflection boundary conditions are used on the upper and lower boundaries, while out flow boundary conditions on are used on the left and right boundaries. The bubble is assumed to be in both thermal and mechanical equilibrium with the surrounding air. The non-dimensionalized initial data are

$$W = (\rho = 1.0,\, u = 0.0,\, p = 1.0, \gamma = 1.4,\, C_v = 0.72)\,, \text{pre-shoc air}$$
$$W = (\rho = 1.36931,\, u = -0.178598,\, p = 1.55603, \gamma = 1.4,\, C_v = 0.72)\,, \text{post-shoc air}$$
$$W = (\rho = 0.1358,\, u = 0.0,\, p = 1.0, \gamma = 1.67,\, C_v = 2.42)\,, \text{helium}\,.$$

Although the density in the bubble region is low, it is still stable. The results are shown in Figure 10.

Problem 7: Explosion in a box:

In this example we consider a helium gas with high pressure in a small box of sides length 0.2 at the center of a large box of unit length containing air. The outer box has reflecting walls. Initially the velocities are zero. The pressure of helium gas is equal 1000 and density equal 1, while air has pressure 10 and density 1. The specific heat ratios for helium and air are 1.67 and 1.4, while specific heats at constant volume are equal to 2.42 and 0.72 respectively. The results are shown in Figure 11.

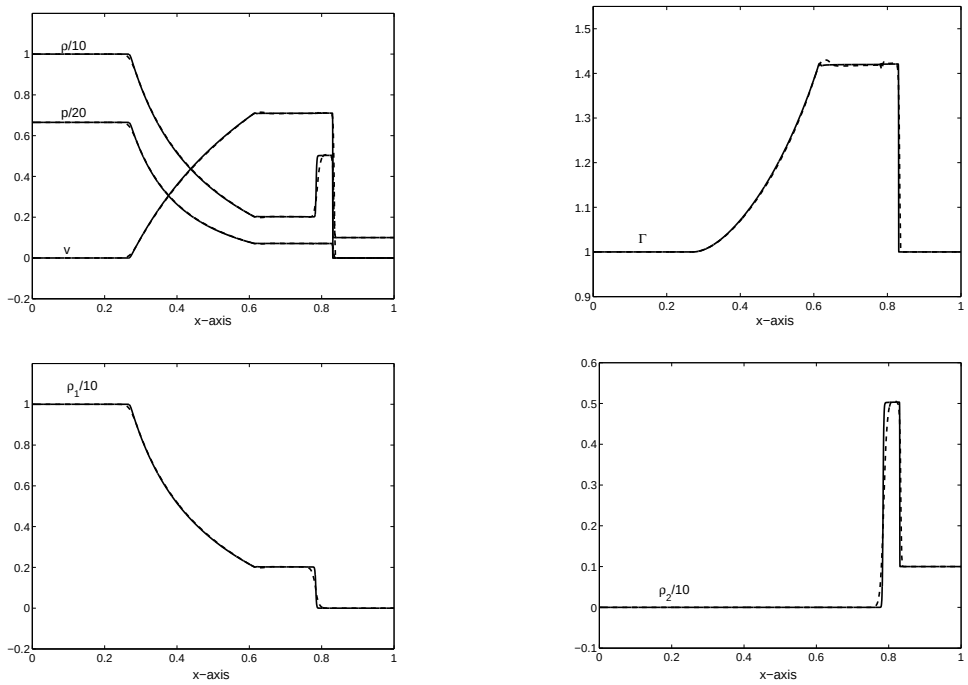

Figure 5: Comparison of problem 1 results with 400 mesh points (Dashed line) versus 4000 points (solid line) at $t = 0.4$.

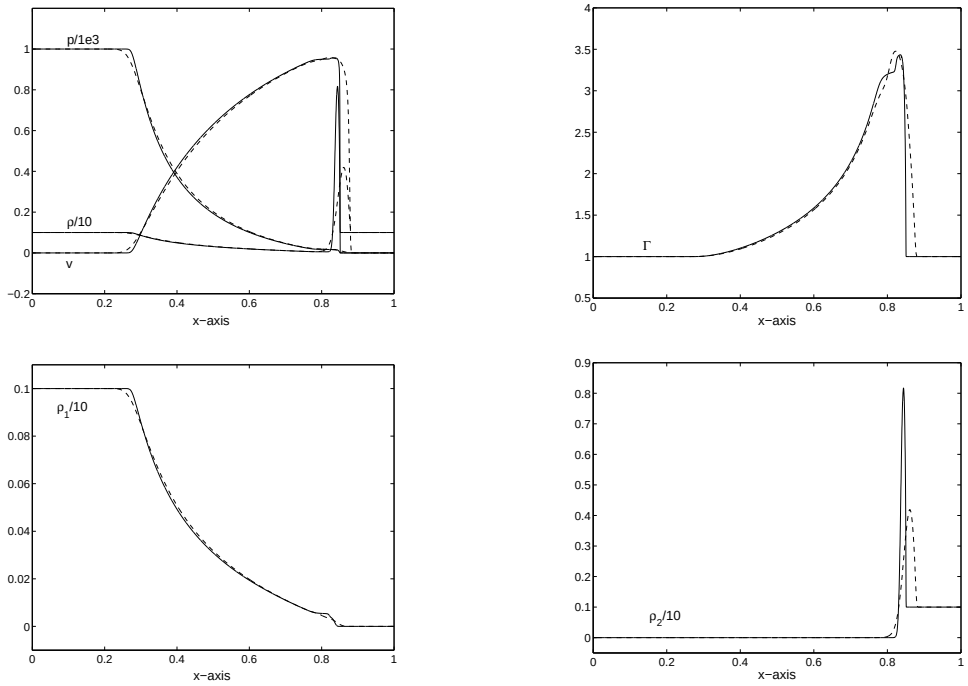

Figure 6: Comparison of problem 2 results with 400 mesh points (Dashed line) versus 4000 points (solid line) at $t = 0.35$.

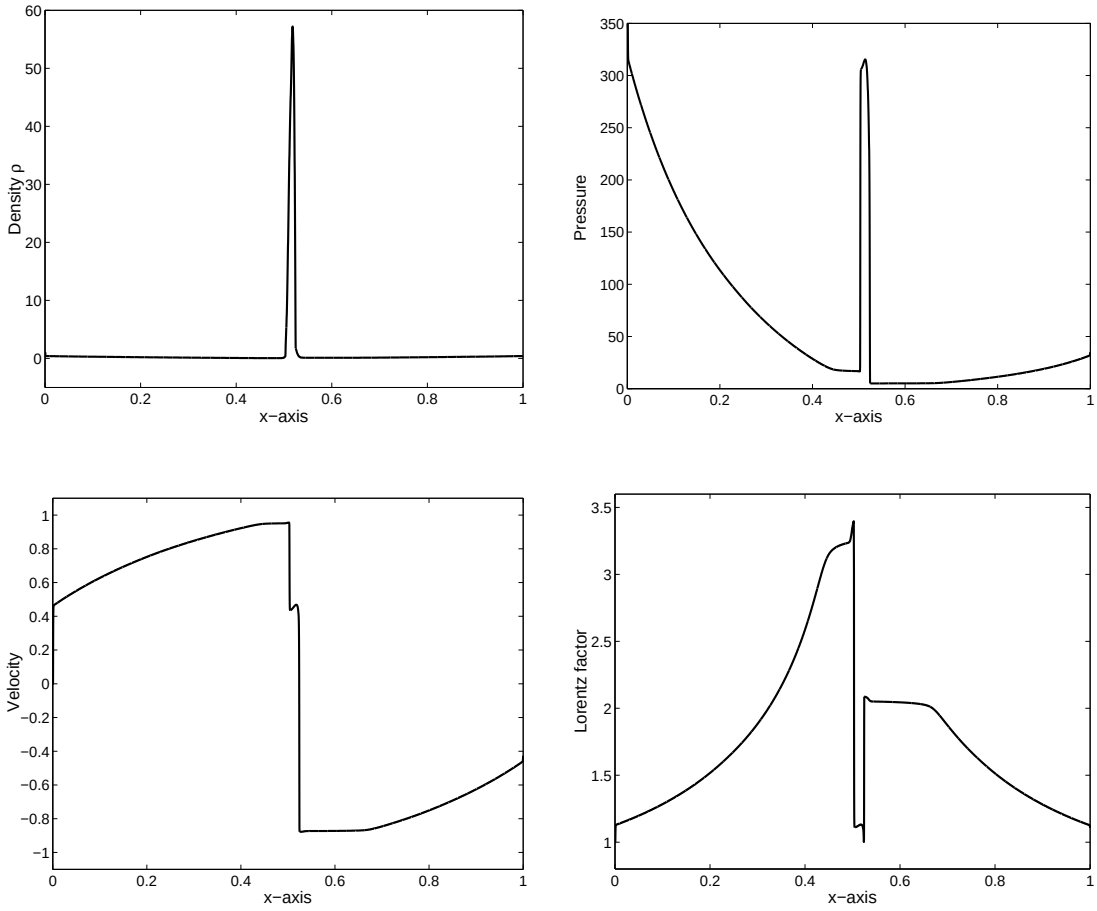

Figure 7: Problem 3 results using 4000 points at $t = 0.43$.

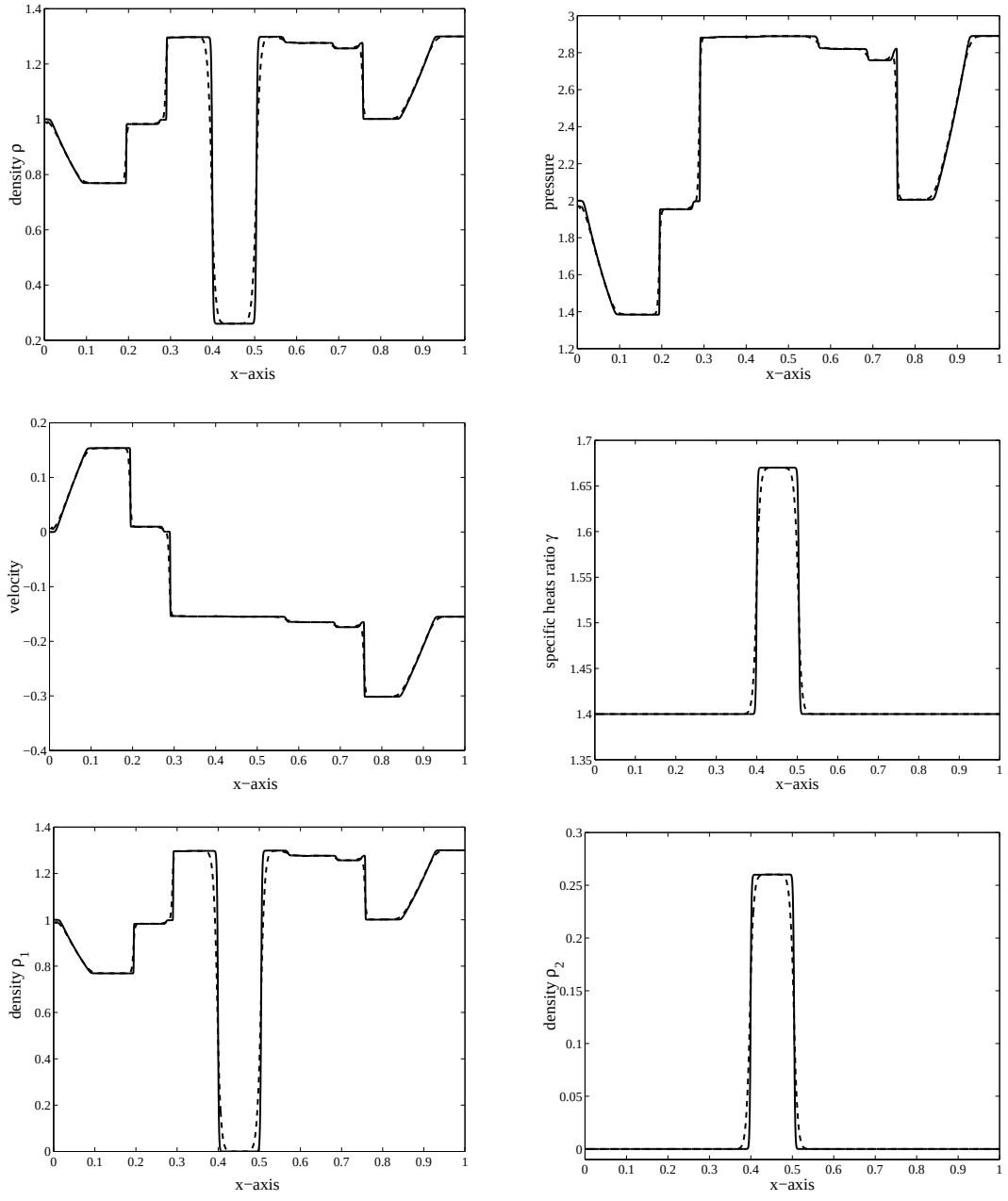

Figure 8: Problem 4 results using 4000 points at $t = 0.7$.

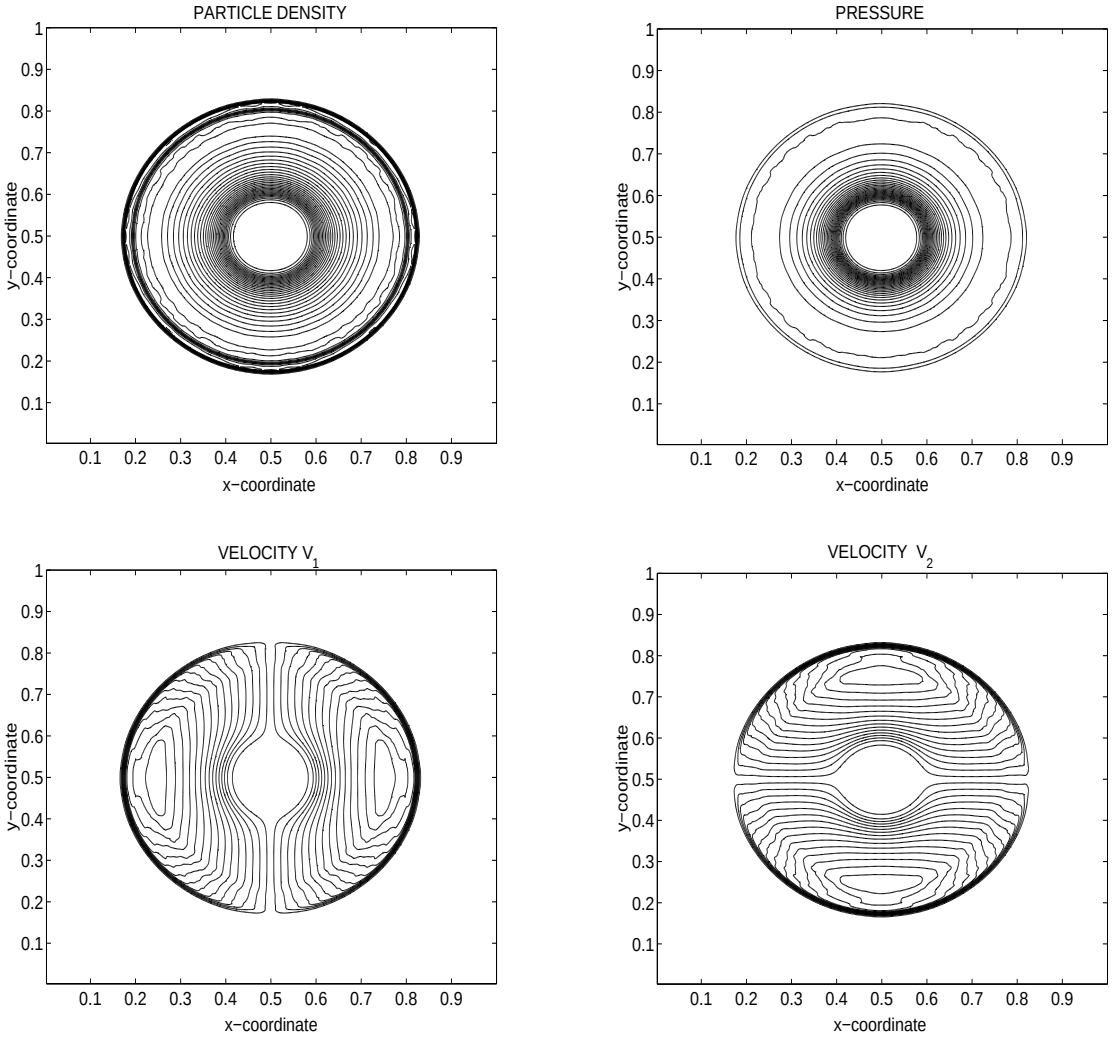

Figure 9: Cylinderical explosion results using 400×400 mesh points at $t = 0.15$.

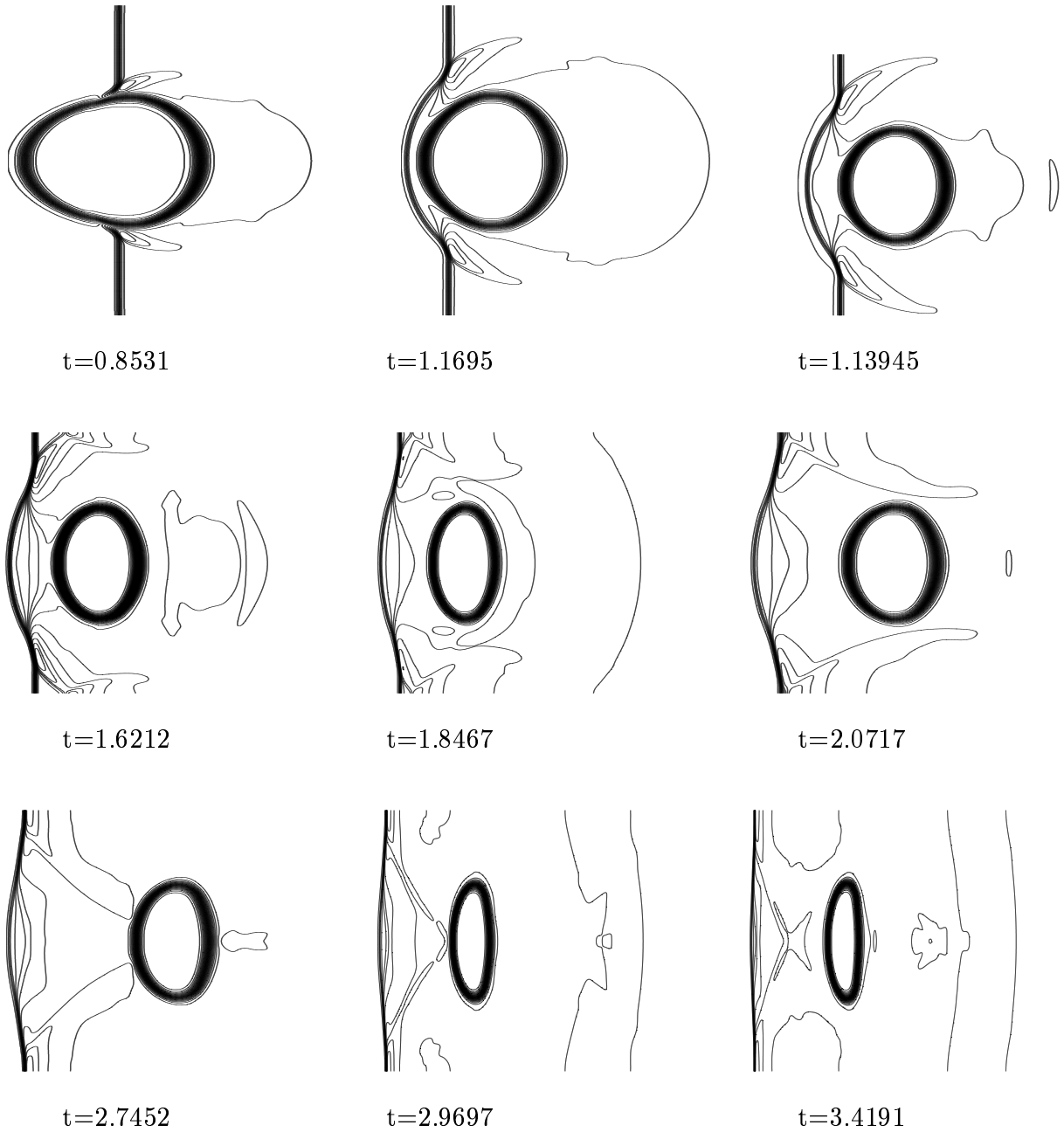

Figure 10: Shock and helium bubble interaction at different times

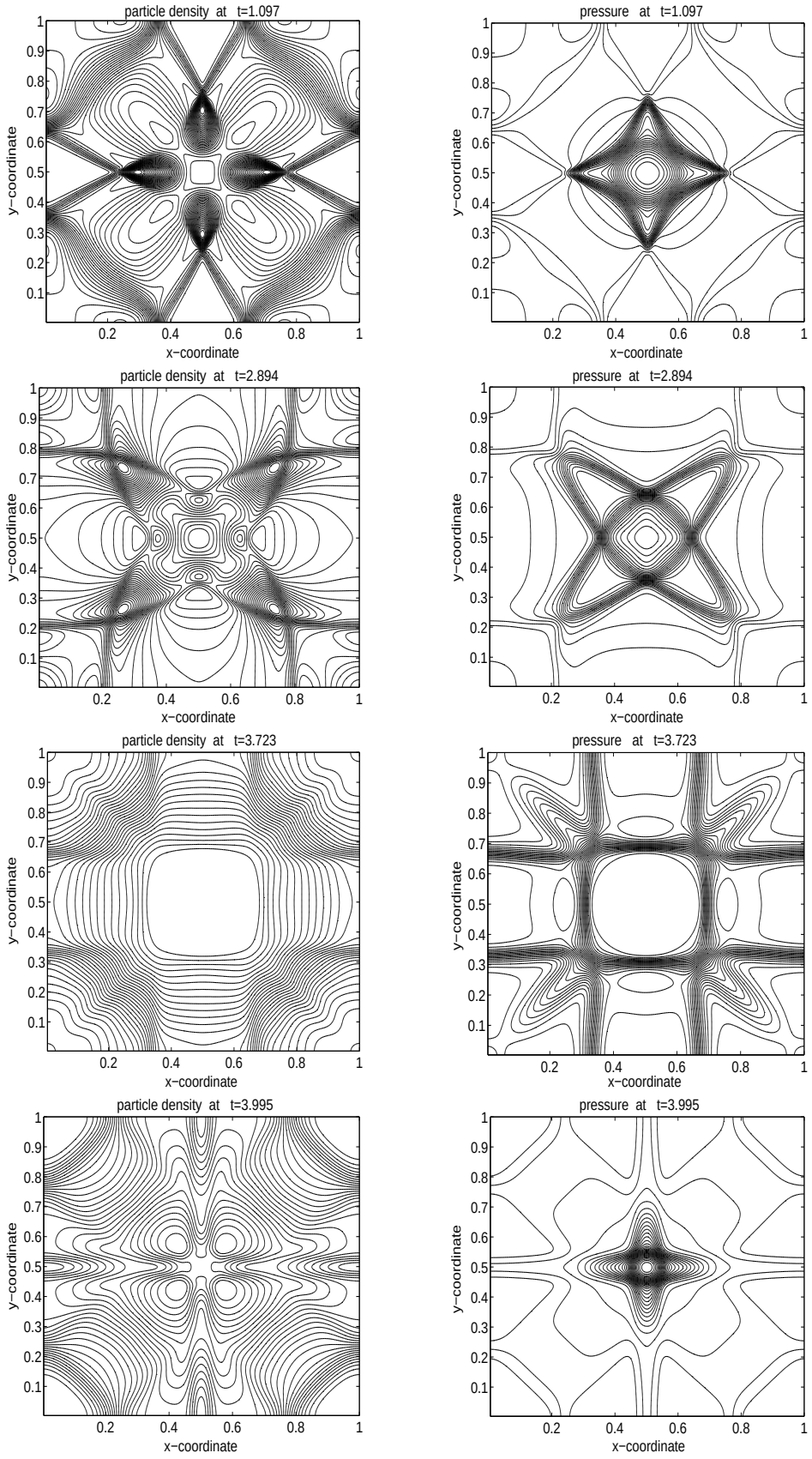

Figure 11: Explosion in a box problem at different times

References

[1] M.A. Aloy, J.M^{a} Ibáñez, J.M^{a} Martí, E. Müller, *GENESIS: A High-Resolution Code for 3D Relativistic Hydrodynamics*, Astrophys. J., **122** (1999), pp. 151-166.

[2] J. Centrella, J.R. Wilson, *Planar Numerical Cosmology II: The Difference Equations and Numerical Tests*, Astrophys. J., **54** (1984), pp. 229-249.

[3] P. Colella, P.R. Woodward, *The Piecewise Parabolic Method (PPM) for Gas-Dynamical Simulations*, J. Comp. Phys., **54** (1993), pp. 174-201.

[4] D.J. Dean, C. Bottcher, M.R. Strayer, *Spline Techniques for Solving Relativistic Equations*, Int. J. Mod. Phys., **C4** (1993), pp. 723-747.

[5] R. Donat, A. Marquina, *Capturing Shock Reflections: An Improved Flux Formula*, J. Comp. Phys., **125** (1996), pp. 42-58.

[6] F. Eulderink, *Numerical Relativistic Hydrodynamics*, PhD thesis, (Rijks-univerteit te Leiden, Leiden, Holland, 1993).

[7] F. Eulderink, and G. Mellema, *General Relativistic Hydrodynamics with a Roe Solver*, Astron. Astrophys. Suppl., **110** (1995), pp. 587-623.

[8] R.P. Fedkiw, T. Aslam, B. Merriman, and S. Osher, *A Non-oscillatory Eulerian Approach to Interfaces in Mathematical Flows (The Ghost Fluid Method)*, J. Comput. Phys, **152**, (1999), pp. 457-492.

[9] R.P. Fedkiw, X.D. Liu, and S. Osher, *A General Technique for Elimination of Spurious Oscillations in Conservative Scheme for Multi-phase and Multi-species Euler Equations*, UCLA CAM Report 97-27 (1997).

[10] J. Glimm, *Solution in the Large for Nonlinear Hyperbolic Systems of Equations*, Commun. Pure Appl. Math., **18** (1965), pp. 697-715.

[11] A. Harten, P.D. Lax, B. van Leer, *On Upstream Differencing and Godunov-Tyoe Schemes for Hyperbolic Conservation Laws*, SIAM Rev., **25** (1983), pp. 35-61.

[12] J.F. Hawley, L.L. Smarr, and J.R. Wilson, *A Numerical Study of Nonspherical Black Hole Accretion. II. Finite Differencing and Code Calibration*, Astrophys. J. Suppl,, **55** (1984), pp. 211-246.

[13] G.-S. Jaing, E. TadMor, *Nonoscillatory Central Schemes for Multidimensional Hyperbolic Conservation Laws*, SIAM J. Sci. Comput. **19** (1998), pp. 1892-1917.

[14] S. Karni, *Viscous Shock Profiles and Premitive Formulations*, SIAM J. Numer. Anal., **29**, (1992), pp.1592-1609.

[15] S. Karni, *Multicomponent Flow Calculations by a Consistent Primitive Algorithm*, J. Comput Phys., **112**, (1994), pp. 31-43.

[16] S. Karni, *Hybrid Multifluid Algorithms*, SIAM J. Sci. Compute, **17**, (1996), pp. 1019-1039.

[17] A. Königl, *Relativistic gasdynamics in two dimension*, Physics of Fluids, **23** (1980), pp. 1083-1090.

[18] Y. Lian and K. Xu, *A Gas-kinetic Scheme for Multimaterial Flows and its Application in Chemical Reaction*, ICASE Report No. 99-28 (1999).

[19] A. Marquina and Pep Mule, *A Flux-split Algorithm Applied to Conservative Model for Multicomponent Compressible Flows*, GrAN report 02-01 (2002).

[20] J.M^{a} Martí, E. Müller, J.A. Font, J.M^{a} Ibáñez, *Morphology and Dynamics of Highly Supersonic Relativistic Jets*, Astrophysics. J., **448** (1995), pp. L105-L108.

[21] J.M^{a} Martí, E. Müller, *Extension of the Piecewise Parabolic Method to one-Dimensional Relativistic Hydrodynamics*, J. Comp. Phys., **123** (1996), pp. 1-14.

[22] J.M^{a} Martí, E. Müller, J.A. Font, J.M^{a} Ibáñez, and A. Marquina, *Morphology and Dynamics of Relativistic Jets*, Astrophysics. J., **479** (1997), pp. 151-163.

[23] J.M^{a} Martí, E. Müller, *Numerical Hydrodynamics in Speical Relativity*, Living Reviews in Relativity, **2** (1999), p. 1-101.

[24] H. Nessayahu, E. Tadmor, *Nonoscillatory Central Differencing for Hyperbolic Conservation Laws*, SIAM J. Comput. Phys., **87** (1990), pp. 408-448.

[25] J. von Neumann, R.D. Richtmyer, J. Appl. Phys., **21** (1950), p. 232.

[26] M.L. Norman, K.-H.A. Winkler, *Why ultrarelativistic Hydrodynamics is Difficult*, in: Astrophysical Radiation Hydrodynamics, eds. M.L. Normnanand K,-H.A. Winkler, Reidel, Dordrecht, (1986), pp. 449-476.

[27] J.J. Quirk and S. Karni, *In the Dynamics of a Shock Bubble Interaction*, J. Fluid Mech., **318**, (1996), pp. 129.

[28] P.L. Rao, *Approximate Riemann Solvers, Parameter Vectors and Difference Schemes*, J. Comp. Phys., **43** (1981), pp. 357-372.

[29] R.H. Sanders, K.H. Prendergast, *The Possible Relation of the 3-Kiloparsec Arm to Explosions in the Galactic Nucleus*, Astrophysics, **188**, (1974), pp. 489-500.

[30] V. Schneider, U. Katscher, D. H. Rischke, B. Waldhauser, J.A. Maruhn, C.-D. Munz, *New Algorithms for Ultra-relativistic Numerical Hydrodynamics*, J. Comp. Phys., **105**, (1993), pp. 92-107.

[31] J. Sollfrank, P. Huovinen, M. Kataja, P.V. Ruuskanen, M. Prakash, R. Venugopalan, *Hydrodynamical Description of 200A GeV/cS + Au Collisions: Hadron and Electromagnetic Spectra*, Phys. Rev., **C55**, (1997), pp. 392-410.

[32] L. Wen, A. Panaitescu, and P. Laguna, *A Shock-Patching Code for Ultra-relativistic Fluid Flows*, Astrophysics. J., **486**, (1997), pp. 919-927.

[33] J.R. Wilson, *A Numerical Study of Fluid Flows in a Kerr Space*, Astrophysics. J., **173**, (1972), pp. 431-438.

[34] J.R. Wilson, *A Numerical Method for Relativistic Hydrodynamics*, in: Sources of Gravitational Radiation, ed. L.L. Smarr, Cambridge University Press, Cambridge, (1972), pp 423-446.

[35] P.R. Woodward, and P. Colella, *The Numerical Simulation of Two-Dimensional Fluid Flow with Strong Shocks*, J. Comp. Phys., **54**, (1984), pp. 115-173.

[36] K. Xu, *BGK-based Scheme for Multicomponent Flow Calculations*, J. Comput Phy., **134** , (1997), pp. 122-133.

[37] K. Xu, *Gas Evolution Dynamics in Godunov-type Schemes and Analysis of Numerical Shock Instability*, ICASE Report No. Tr. 99-6, (1998).

[38] J.Y. Yang, M.H. Chen, I-N. Tsai, J.W. Chang, *A Kinetic Beam Scheme for Relativistic Gas Dynamics*, J. Comput. Phys., **136**, (1997), pp. 19-40.